IJMMM International Journal of Minerals, Metallurgy and Materials 矿物冶金与材料学报（英文版）

Fabrication and properties of silver-based composites reinforced with carbon-coated Ti_3AlC_2

Yong-fa Zhu, Wu-bian Tian, Dan-dan Wang, Heng Zhang, Jian-xiang Ding, Pei-gen Zhang, and Zheng-ming Sun

Cite this article as:
Yong-fa Zhu, Wu-bian Tian, Dan-dan Wang, Heng Zhang, Jian-xiang Ding, Pei-gen Zhang, and Zheng-ming Sun, Fabrication and properties of silver-based composites reinforced with carbon-coated Ti_3AlC_2, *Int. J. Miner. Metall. Mater.*, 28(2021), No. 11, pp. 1836-1843. https://doi.org/10.1007/s12613-020-2064-6

View the article online at SpringerLink or IJMMM Webpage.

Articles you may be interested in

Yu-peng Li, Da-qian Sun, Wen-biao Gong, and Liang Liu, Effects of postweld aging on the microstructure and properties of bobbin tool friction stir-welded 6082-T6 aluminum alloy, *Int. J. Miner. Metall. Mater.*, 26(2019), No. 7, pp. 849-857. https://doi.org/10.1007/s12613-019-1800-2

Li Zhang, Bao-lin Wu, and Yu-lin Liu, Microstructure and mechanical properties of a hot-extruded Al-based composite reinforced with core-shell-structured Ti/Al_3Ti, *Int. J. Miner. Metall. Mater.*, 24(2017), No. 12, pp. 1431-1437. https://doi.org/10.1007/s12613-017-1536-9

Li Xiao, Pei-wei Han, Yong-liang Wang, Guo-yan Fu, Zhi Sun, and Shu-feng Ye, Silver dissolution in a novel leaching system: Reaction kinetics study, *Int. J. Miner. Metall. Mater.*, 26(2019), No. 2, pp. 168-177. https://doi.org/10.1007/s12613-019-1721-0

Shahab Shahsavar, Mostafa Ketabchi, and Saeed Bagherzadeh, Fabrication of robust aluminum–carbon nanotube composites using ultrasonic assembly and rolling process, *Int. J. Miner. Metall. Mater.*, 28(2021), No. 1, pp. 160-167. https://doi.org/10.1007/s12613-020-1969-4

Ze-cheng Hou, Lun-qiao Xiong, Yuan-feng Liu, Lin Zhu, and Wen-zhen Li, Preparation of super-aligned carbon nanotube-reinforced nickel-matrix laminar composites with excellent mechanical properties, *Int. J. Miner. Metall. Mater.*, 26(2019), No. 1, pp. 133-141. https://doi.org/10.1007/s12613-019-1717-9

Hua-ping Sun, Jun Wu, Tian Tang, Bo Fan, and Zheng-hua Tang, Effect of vanadium carbide on commercial pure aluminum, *Int. J. Miner. Metall. Mater.*, 24(2017), No. 7, pp. 833-841. https://doi.org/10.1007/s12613-017-1467-5

IJMMM WeChat

QQ author group

International Journal of Minerals, Metallurgy and Materials
Volume 28, Number 11, November 2021, Page 1836
https://doi.org/10.1007/s12613-020-2064-6

Fabrication and properties of silver-based composites reinforced with carbon-coated Ti_3AlC_2

Yong-fa Zhu[1)], *Wu-bian Tian*[1)], *Dan-dan Wang*[1)], *Heng Zhang*[1)], *Jian-xiang Ding*[1,2)], *Pei-gen Zhang*[1)], *and Zheng-ming Sun*[1)]

1) Jiangsu Key Laboratory of Advanced Metallic Materials, School of Materials Science and Engineering, Southeast University, Nanjing 211189, China
2) Key Laboratory of Metallurgical Emission Reduction & Resources Recycling, Ministry of Education, School of Materials Science and Engineering, Anhui University of Technology, Ma'anshan 243002, China
(Received: 13 March 2020; revised: 1 April 2020; accepted: 7 April 2020)

Abstract: Ti_3AlC_2-reinforced Ag-based composites, which are used as sliding current collectors, electrical contacts, and electrode materials, exhibit remarkable performances. However, the interfacial reactions between Ag and Ti_3AlC_2 significantly degrade the electrical and thermal properties of these composites. To diminish these interfacial reactions, we fabricated carbon-coated Ti_3AlC_2 particles (C@Ti_3AlC_2) as reinforcement and prepared Ag–10wt%C@Ti_3AlC_2 composites with carbon-layer thicknesses ranging from 50–200 nm. Compared with the uncoated Ag–Ti_3AlC_2 composite, Ag–C@Ti_3AlC_2 was found to have a better distribution of Ti_3AlC_2 particles. With increases in the carbon-layer thickness, the Vickers hardness value and relative density of Ag–C@Ti_3AlC_2 gradually decreases. With a carbon-layer thickness of 150 nm, we obtained the lowest resistivity of Ag–C@Ti_3AlC_2 of 29.4 135.5×10^{-9} Ω·m, which is half that of Ag–Ti_3AlC_2 (66.7×10^{-9} Ω·m). The thermal conductivity of Ag–C@Ti_3AlC_2 reached a maximum value of 135.5 $W\cdot m^{-1}\cdot K^{-1}$ with a 200-nm carbon coating (~1.8 times that of Ag–Ti_3AlC_2). These results indicate that the carbon-coating method is a feasible strategy for improving the performance of Ag–C@Ti_3AlC_2 composites.

Keywords: silver-based composite; titanium aluminum carbide; carbon coating; interfacial reaction; properties

1. Introduction

MAX (short for $M_{n+1}AX_n$) phases are a class of layered ternary compounds, in which M is an early transition metal, A is an IIIA to ⅥA element, and X is either carbon or nitrogen [1–2]. These compounds are attractive and promising materials for structural, thermal, and electrical applications, due to their combined ceramic and metal properties, including low density, high modulus and strength, high electrical conductivity, good thermal conductivity, low coefficient of friction, good thermal stability, and oxidation resistance [2].

Ti_3AlC_2, as a representative MAX phase, has low density (4.21 $g\cdot cm^{-3}$) [3], relatively low hardness (HV ~3.5 GPa) [3–4], good thermal conductivity (40 $W\cdot m^{-1}\cdot K^{-1}$), and high electrical conductivity (3.48×10^6 $\Omega^{-1}\cdot m^{-1}$) [2–3]. Such unique properties make Ti_3AlC_2 a promising reinforcement material in Ag-based composites, which are frequently used as sliding current collectors, electrical contacts, and electrode materials [5]. However, in the Ag–Ti_3AlC_2 composite, dramatic interfacial reactions occur between the Ag and Ti_3AlC_2 particles during sintering at high temperatures. According to Liu *et al*. [6], the interfacial structure is changed by the de-intercalation of the Al atom from Ti_3AlC_2 followed by Al diffusion into the Ag lattice, which forms a new layer comprising a TiC_x compound and an Ag(Al) solid solution. In addition to the Ag–Ti_3AlC_2 composite, other metal/MAX systems have been reported to experience similar interfacial reactions, including Al–Ti_3SiC_2 [7–8], Cu–Ti_3SiC_2 [9], Cu–Ti_3AlC_2 [10], and Ag–Ti_2SnC [11].

For metal–MAX composites, the interfacial condition between different components can be optimized to significantly enhance the mechanical properties [12–13]. In addition, the interfacial reaction could improve the wetting behavior between the metal and MAX phases [14–15]. However, the formation of new phases at the interface can deteriorate the interfacial structure and electrical properties [16]. One feasible approach for tailoring the interfacial structure is to modify the surface condition of the MAX phase. Zhou *et al.* [17]

Corresponding authors: Wu-bian Tian E-mail: wbtian@seu.edu.cn; Zheng-ming Sun E-mail: zmsun@seu.edu.cn
© University of Science and Technology Beijing 2021

successfully prepared Cu-coated Ti_3SiC_2 (Cu@Ti_3SiC_2) to reinforce Cu-matrix composites, and reported the density and mechanical properties of the Cu–Cu@Ti_3SiC_2 composite to be superior to those of the uncoated composite. Wang *et al.* [18] fabricated Al–Cu@Ti_3SiC_2 composites and found that improved wetting leads to better mechanical and tribological properties.

Inspired by these results, we proposed that the formation of a protective carbon layer around Ti_3AlC_2 particles may obstruct direct contact between the Ag and Ti_3AlC_2 components, and thus prevent any interfacial reaction at the boundary. We selected carbon materials for this study due to their excellent properties that include good electrical conductivity and chemical and thermal stabilities [19–20]. Phenol-formaldehyde resin is one of the most commonly used carbon precursors, due to its outstanding physicochemical properties of good carbon yield, easy functionalization, and thermal stability.

In this study, we utilized Ti_3AlC_2 particles coated with a layer of carbon as reinforcement for the Ag matrix (Ag–C@Ti_3AlC_2), and then we investigated the interfacial structure. For comparison, we synthesized Ag–C@Ti_3AlC_2 composites with carbon layers of different thicknesses. The density and mechanical, electrical, and thermal properties of Ag–C@Ti_3AlC_2 composites were then studied and analyzed to clarify the role of the carbon coating.

2. Experimental

2.1. Synthesis of Ti_3AlC_2 and carbon-coated Ti_3AlC_2 powders

The raw materials used to synthesize Ti_3AlC_2 include commercially available Ti (~300 mesh, 99.7%), Al (~300 mesh, 99.7%), and TiC (2~4 μm, 99.9%) powders. The Ti_3AlC_2 (99.0%) was prepared from a 1.8Ti: 1Al: 1TiC powder mixture (atomic ratio) by pressureless sintering at 1450°C for 2 h and then milling to a size of approximately 5 μm.

Table 1 lists the compositions of the chemicals used in the carbon-coating procedure of the Ti_3AlC_2 particles. Fig. 1 shows a flow chart of the *in-situ* formation of the carbon layer on the surface of a Ti_3AlC_2 particle. In the synthesis of phenolic resin [21], formaldehyde is slowly added dropwise into a resorcinol and Ti_3AlC_2 solution. Because the coating reaction must occur under alkaline conditions, we added a certain amount of ammonia as a pH regulator [19]. The whole reaction process was conducted in a magnetic stirring flask for 24 h at room temperature. Then, the resin-coated Ti_3AlC_2 powder was washed with deionized water and alcohol several times before being dried in a drying container overnight. The phenolic resin was carbonized at 700°C for 5 h to finally obtain carbon-coated Ti_3AlC_2 particles (C@Ti_3AlC_2). The thickness of the carbon layer can be controlled by adjusting the ratio of resorcinol to formaldehyde and the pH value during the reaction process. In the experiments, we achieved average carbon-layer thicknesses ranging from 50 to 200 nm.

2.2. Synthesis of Ag–C@Ti_3AlC_2 composites

As in our previous work on Ag–Ti_3AlC_2 composites [22], to reinforce the Ag matrix, C@Ti_3AlC_2 particles with carbon layers of different thicknesses were used. Ag (99.9%, ~10 μm) and 10wt% reinforcement particles were mixed by wet-ball milling in alcohol solution for 0.5 h at a rotation speed of 250 r/min [23]. The ball-to-powder and alcohol-to-powder mass ratios were 3:2 and 1:1, respectively. After being dried in the drying container at 60°C for 24 h, the mixed powders were pressed into graphite molds with a diameter of 20 mm. The spark plasma sintering (SPS) technique was then used to densify these powder mixtures at 800°C for 20 min under 50 MPa.

2.3. Characterization

The thickness of the carbon layers was measured with a transmission electron microscope (TEM, G220, FEI). The phase constituents of the sintered samples were examined by X-ray diffraction (XRD, Smartlab 3, Rigaku). Wire machining was used to cut the prepared samples into specimens with the dimensions 1 mm × 1 mm × 15 mm. The electrical resistivity was measured using a four-point-probe ohmmeter (MetraHit27I, GMC). After being placed under a 1-kg load for 10 s, the Vickers hardness values of the specimens were

Table 1. Compositions of the chemicals used in the carbon coating procedure of Ti_3AlC_2 particles

Ti_3AlC_2	Alcohol	Deionized water	Resorcinol ($C_6H_4(OH)_2$)	Formaldehyde (HCHO)	Ammonia ($HNO_3 \cdot H_2O$)
20 g/L	500 mL/L	500 mL/L	2–8 g/L	7–28 mL/L	1–4 mL/L

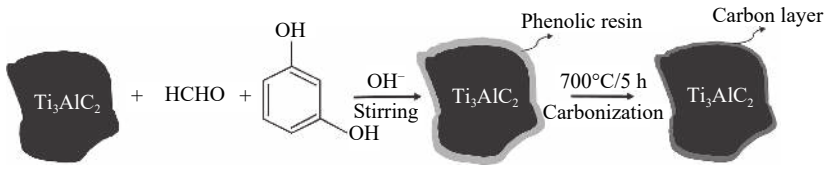

Fig. 1. Flow chart of the *in-situ* formation of a carbon layer on the Ti_3AlC_2 particle surface.

measured using a micro-hardness tester (FM-700, Future-Tech). The densities of the composites were measured using the Archimedes method (DH-300, Reeko Instrument Co., Ltd.). The theoretical densities of the composites were calculated by the rule of mixture using the theoretical densities of the C@Ti_3AlC_2 and Ag phases. For example, according to the calculation model, for a thickness of 200 nm, the volume content of carbon accounts for 20% of the total volume in C@Ti_3AlC_2. The interfacial microstructures were characterized using a field-emission scanning electron microscope (FE-SEM, FEI/Philips Sirion 2000, Netherlands) equipped with an energy dispersive spectrometer (EDS, AZtec XMAX80).

3. Results and discussion

3.1. TEM observations of as-sintered Ti_3AlC_2 and C@Ti_3AlC_2 particles

Figs. 2(a)–2(c) show TEM microstructure photographs of the as-sintered and carbon-coated Ti_3AlC_2 particles. The photograph in Fig. 2(a) shows an uncoated Ti_3AlC_2 particle with a diameter of approximately 5 μm. As labelled in Fig. 2(b), the black and light gray areas are the Ti_3AlC_2 matrix and carbon layer, respectively. As shown in Fig. 2(c), the carbon layer has a uniform thickness of approximately 100 nm and is tightly wrapped around the Ti_3AlC_2 particle. The carbon content can be roughly calculated with reference to a schematic diagram after determining the layer thickness, as shown in Fig. 2(d). In addition to the carbon coating around the Ti_3AlC_2, there are some residual and free carbons, which can be removed in a subsequent washing procedure.

3.2. Microstructure of Ag–Ti_3AlC_2 and Ag–C@Ti_3AlC_2 composites

The distribution of the reinforcement phase in composites greatly influences their microstructure and performance. Figs. 3(a) and 3(b) show SEM images of the Ag–Ti_3AlC_2 and Ag–C@Ti_3AlC_2 composites prepared by the SPS method, in which the light-gray and dark-gray phases are Ag and Ti_3AlC_2, respectively. Compared with the Ag–C@Ti_3AlC_2 composite (Fig. 3(b)), some aggregations of the Ti_3AlC_2 phase and blocks of the Ag matrix are evident in the Ag–Ti_3AlC_2 sample (arrows in Fig. 3(a)). This suggests that the carbon-layer-wrapped Ti_3AlC_2 particles are uniformly

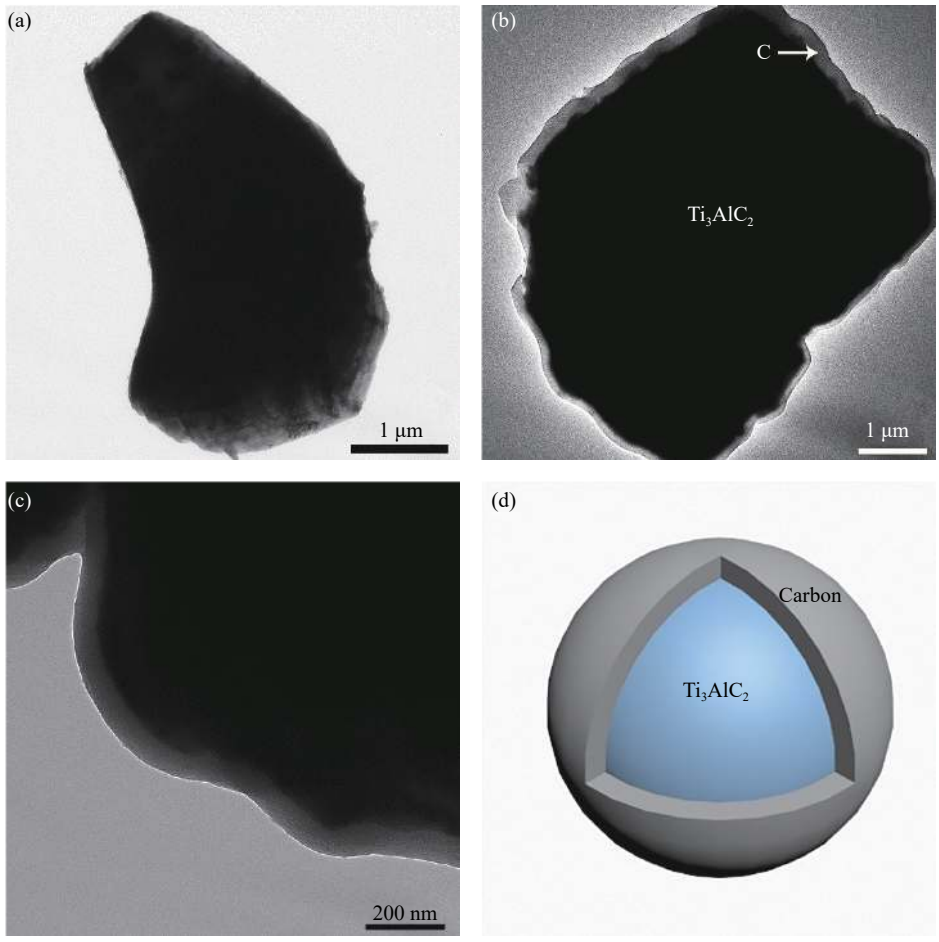

Fig. 2. Microstructure of (a) Ti_3AlC_2 particle and (b, c) carbon-coated Ti_3AlC_2 particle at different magnifications, and (d) schematic diagram of C@Ti_3AlC_2 structure.

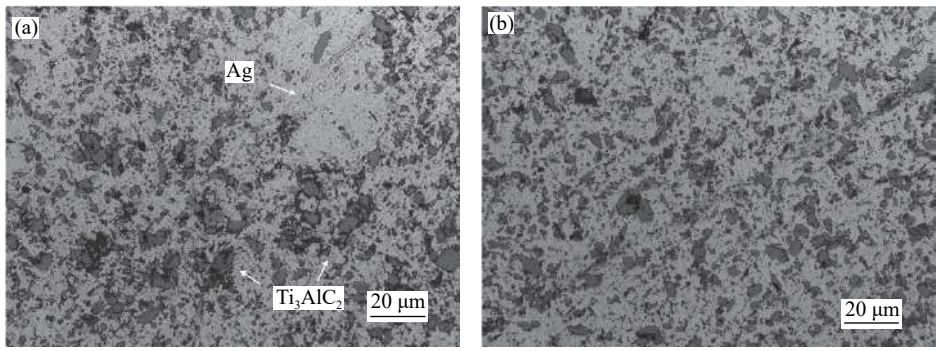

Fig. 3. Microstructure of the (a) Ag–Ti_3AlC_2 and (b) Ag–C@Ti_3AlC_2 composites prepared by SPS.

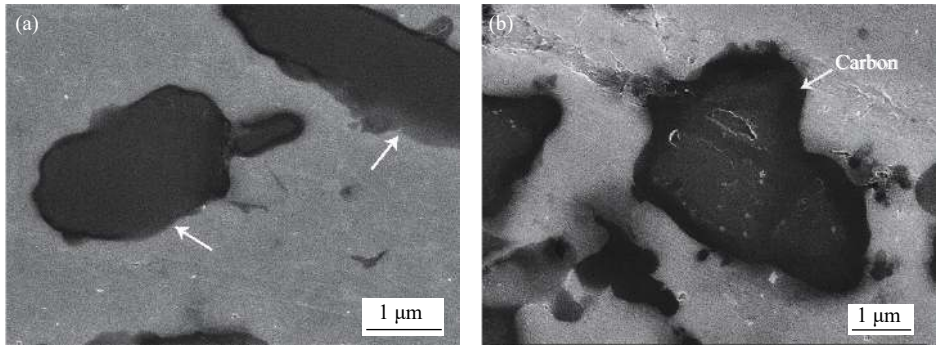

Fig. 4. Microstructure of Ag–C@Ti_3AlC_2 composites at high magnification with carbon thicknesses of (a) 50 nm and (b) 200 nm.

dispersed in the Ag–C@Ti_3AlC_2 composite.

Fig. 4 shows the microstructure of the Ag–C@Ti_3AlC_2 composite at higher magnifications. As shown in Fig. 4(a), some of the Ti_3AlC_2 particles are in direct contact with the Ag matrix with the 50-nm carbon coating (marked by white arrows), which may be due to breakage of the coating during the mixing process. When the carbon thickness was increased to 200 nm, the Ti_3AlC_2 particles were observed to be wrapped tightly and completely, as shown in Fig. 4(b).

3.3. Phase analysis of Ag–Ti_3AlC_2 and Ag–C@Ti_3AlC_2 composites

The reactions between Ti_3AlC_2 and Ag during the preparation of the Ag–Ti_3AlC_2 composites were identified based on the XRD results. Fig. 5 shows the XRD patterns of the standard Ag (PDF#04-0783), SPSed compacts of Ag–Ti_3AlC_2, and Ag–C@Ti_3AlC_2 with carbon thicknesses of 50, 100, 150, and 200 nm, respectively. All of the samples are mainly composed of Ag and Ti_3AlC_2 phases. However, the strongest Ag (111) peak position in the Ag–Ti_3AlC_2 sample shifted to a high angle of 0.42°, compared with that of the standard Ag, as is clearly shown in the inset in Fig. 5. Without the covering of the carbon layer, Al atoms from the Ti_3AlC_2 diffuse easily into the Ag lattice to partially substitute for the Ag atoms during sintering, forming an Ag(Al) solid solution. The lattice parameter of pure Al (0.40494 nm) is smaller than that of Ag (0.40862 nm), which reduces the lattice parameter values of the Ag(Al) solid solution, and hence the higher-angle shift of the Ag peak in the XRD pattern. When the carbon thickness was increased to more than 150 nm, the Ag peaks become consistent with those of standard Ag, which suggests the enhanced stability of Ti_3AlC_2 and the hindered diffusion of Al atoms.

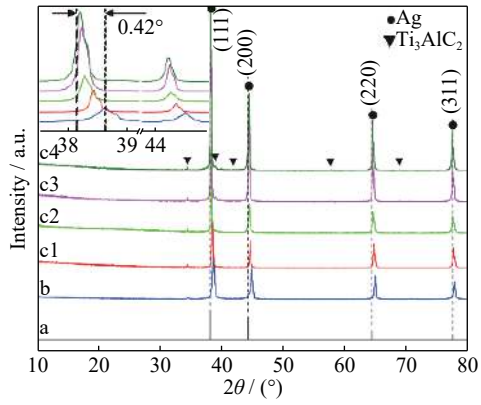

Fig. 5. XRD patterns of (a) standard Ag (PDF#04-0783), (b) Ag–Ti_3AlC_2, and Ag–C@Ti_3AlC_2 with the carbon thicknesses of (c1) 50 nm, (c2) 100 nm, (c3) 150 nm, and (c4) 200 nm.

3.4. Analysis of interfacial reactions of Ag–Ti_3AlC_2 and Ag–C@Ti_3AlC_2 composites

To directly describe the interfacial reaction and investigate the function of the carbon layers, we generated EDS maps to investigate the elemental distributions of the Ag–Ti_3AlC_2 and Ag–C@Ti_3AlC_2 with a 150-nm carbon layer, as shown in

Figs. 6 and 7, respectively. For the Ag–Ti_3AlC_2 sample, the boundaries of the Al and Ag elements have become blurred compared with those of Ti, as shown in Figs. 6(b)–6(e). For spot #1 located inside the Ti_3AlC_2 particle near the interface (Fig. 6(a)), the atomic ratio of Ti to Al (Ti/Al = 3.3) was fairly close to that of Ti_3AlC_2 (Ti/Al = 3) and a large amount of Ag (10.2at%) was detected. For spot #2 located in the Ag matrix near the interface, we observed significant amounts of Ti and Al as well as Ag. The substantial interdiffusion between the Ti_3AlC_2 and Ag matrix accounts for this result. For the Ag–C@Ti_3AlC_2 sample (Fig. 7), the elemental maps of Ag, Ti, and Al show much clearer shapes, and the element C is easily observable around the Ti_3AlC_2 particle in the Ag–C@Ti_3AlC_2 sample in Fig. 7(e). In addition, the atomic ratio of Ti and Al (Ti/Al = 3.03) of spot #1 is almost same as that of Ti_3AlC_2, with only trace Al or Ti elements detected at the edge of the Ag matrix (spot #2). Therefore, the introduction of the carbon layer significantly impeded the interdiffusion process and thus maintained the integrity of the Ti_3AlC_2-phase reinforcement.

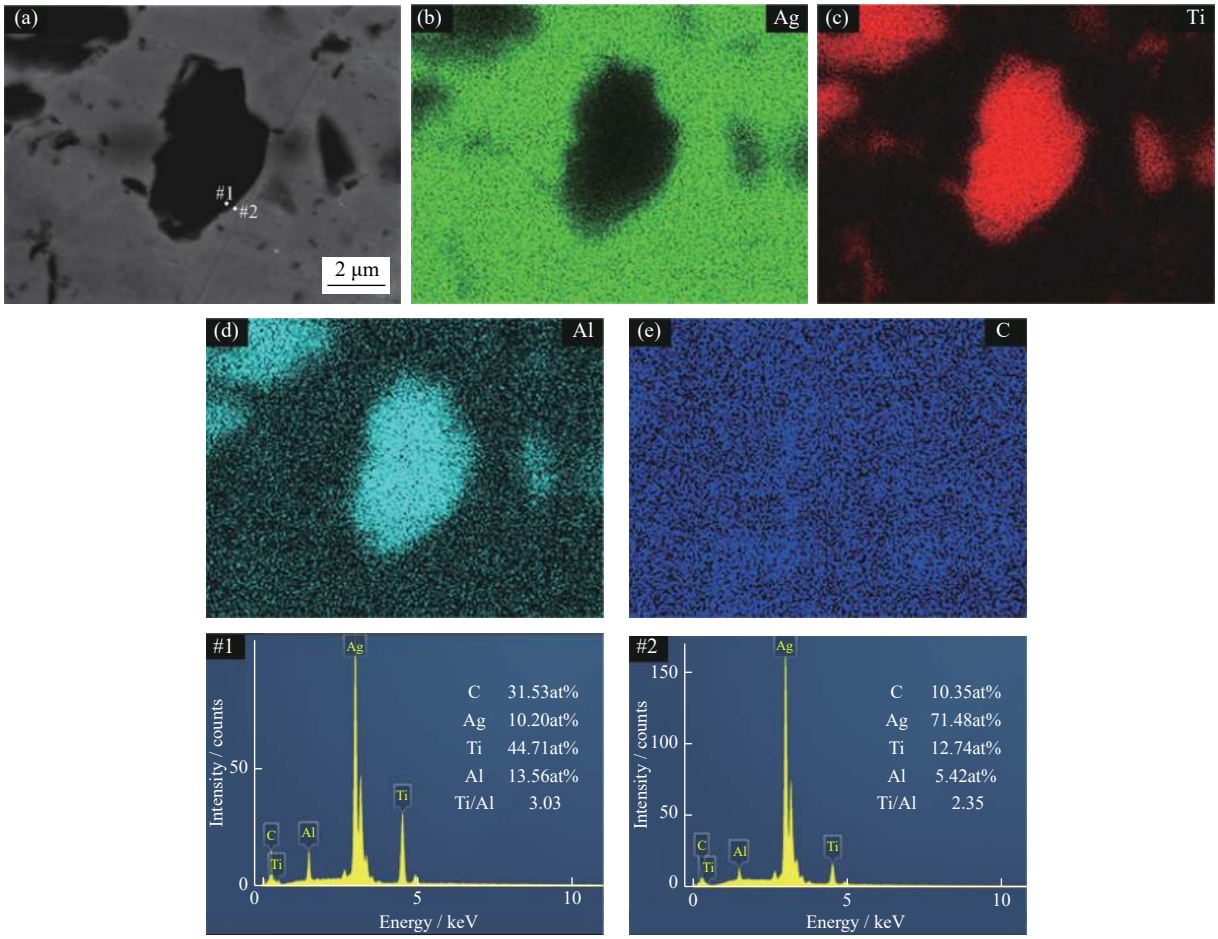

Fig. 6. Element distributions of the Ag–Ti_3AlC_2 composites: (a) SEM image and elemental maps of (b) Ag, (c) Ti, (d) Al, and (e) C. The EDS spectra correspond to spots #1 and #2 in (a), respectively.

3.5. Properties of Ag–Ti_3AlC_2 and Ag–C@Ti_3AlC_2 composites

Composite properties, including mechanical, electrical and thermal properties, are affected by the quantity and distribution of the reinforcements as well as the interfacial state. Changes in the surface state of Ti_3AlC_2, therefore, influence the properties of Ag–C@Ti_3AlC_2 composites. As can be seen in Fig. 8(a), the SPSed Ag–Ti_3AlC_2 composite had a high density of 9.11 g/cm^3. With increases in the thickness of the carbon layer, the densities of the sintered samples gradually decreased. The composite with a 200-nm carbon layer showed a density of 8.33 g/cm^3. The low density of the carbon layer and possibly the poor wettability between Ag and C led to the decrease in the composite density.

As shown in Fig. 8(a), the uncoated Ag–Ti_3AlC_2 had a hardness value of HV 115.6±0.2, which is significantly higher than that (HV 86) of the pressureless sintered sample but slightly lower than that (HV 132) of the sample prepared by equal-channel angular pressing [24]. As the thickness of the carbon layer was increased, the hardness of the Ag–C@Ti_3AlC_2 composite continually decreased. The structural in-

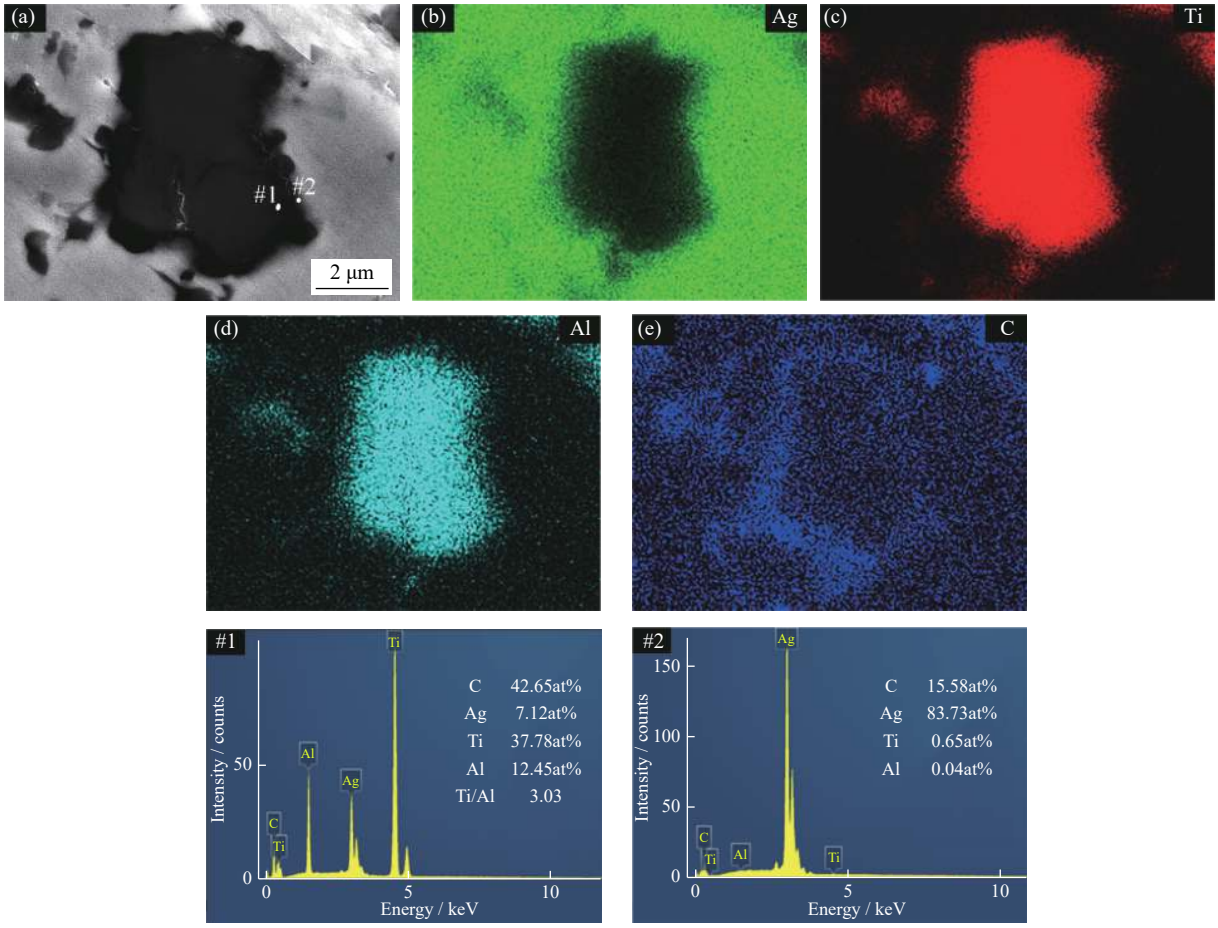

Fig. 7. Element distributions of the Ag–C@Ti_3AlC_2 (150 nm) composites: (a) SEM image and elemental maps of (b) Ag, (c) Ti, (d) Al, and (e) C. The EDS spectra correspond to spot #1 and spot #2 in (a), respectively.

stability at the interface of Ag–Ti_3AlC_2 led to the deintercalation and outward diffusion of Al atoms and the formation of an Ag(Al) solid solution and a TiC_x compound [6,25]. Due to strengthening of the solid solution, the hardness of the Ag(Al) should be greater than that of the original Ag matrix. Therefore, the interfacial reaction products of the Ag–Ti_3AlC_2 composite provide a load-transfer effect during the deformation process, which improves the mechanical properties, i.e., strength and hardness [10,26]. Therefore, we can attribute the decreased hardness of the Ag–C@Ti_3AlC_2 composites to the lack of any interfacial reaction and the decrease in density.

Fig. 8(b) shows the electrical resistivity and thermal conductivity values of the Ag–Ti_3AlC_2 and Ag–C@Ti_3AlC_2

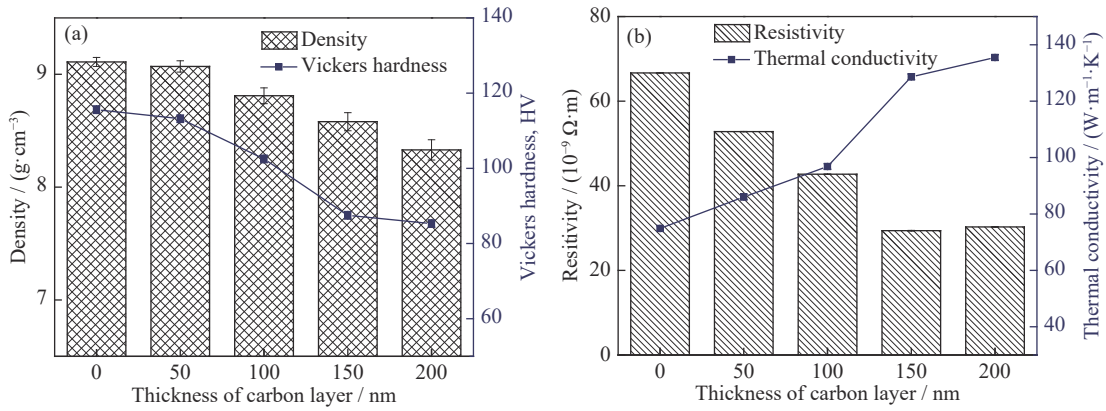

Fig. 8. (a) Density and hardness and (b) resistivity and thermal conductivity values of the Ag–Ti_3AlC_2 and Ag–C@Ti_3AlC_2 composites with carbon layers of different thickness.

composites. The electrical resistivity of the Ag–Ti_3AlC_2 composite was 66.7 × 10^{-9} Ω·m, which is close to the previously reported value (59.3 × 10^{-9} Ω·m) [24]. The resistivities of the Ag–C@Ti_3AlC_2 composites gradually decreased with increases in the thickness of the carbon layer. The lowest electrical resistivity of Ag–C@Ti_3AlC_2 was 29.4 × 10^{-9} Ω·m with a carbon-layer thickness of 150 nm. The thermal conductivity increased from the 74.9 $W·m^{-1}·K^{-1}$ of the uncoated compact to 135.9 $W·m^{-1}·K^{-1}$ of the Ag–C@Ti_3AlC_2 with a 200-nm-thick carbon coating, as shown in Fig. 8(b). A carbon layer hinders the diffusion of the Al element and restrains the formation of the Ag(Al) solid solution zone, which results in reduced electron scattering in the composite and thus improved electrical and thermal conductivities. Undoubtedly, the enhanced integrity of the carbon coating around Ti_3AlC_2 also contributed to these performances.

4. Conclusion

Interfacial reactions in Ag–Ti_3AlC_2 composites degrade their electrical conductivity. In this study, carbon-coated Ti_3AlC_2 was prepared as a reinforcement to modify the interfacial state of the Ag–Ti_3AlC_2 composite. This carbon layer serves as a barrier to interfacial reactions. As the carbon-layer thickness was increased, we found the Vickers hardness of the Ag–10wt%C@Ti_3AlC_2 to decrease because of the absence of the Ag(Al) solid solution and TiC_x compound, as well as the decreased relative density. The lowest resistivity of the Ag–10wt%C@Ti_3AlC_2 was found to be 29.4 × 10^{-9} Ω·m with a carbon-layer thickness of 150 nm, which is much lower than that of the uncoated composite (66.7 × 10^{-9} Ω·m). The highest thermal conductivity of Ag–C@Ti_3AlC_2 with a 200-nm-thick carbon coating reached 135.5 $W·m^{-1}·K^{-1}$, much higher than that (74.9 $W·m^{-1}·K^{-1}$) of the uncoated compact. By combining the processing and properties of Ag–C@Ti_3AlC_2 composites, the optimal thickness of the carbon layer should be in the range of 100–150 nm. These results indicate that carbon coating could be a promising method for adjusting the interfacial structure and improving the electrical and thermal properties of Ag–Ti_3AlC_2 composites.

Acknowledgements

The authors acknowledge the financial support of the National Natural Science Foundation of China (Nos. 51731004 and 51671054), the Natural Science Foundation of Jiangsu Province (No. BK20181285), and the Fundamental Research Funds for the Central Universities, China (No. 2242019K 40056).

References

[1] M.W. Barsoum, The $M_{n+1}AX_n$ phases: A new class of solids: Thermodynamically stable nanolaminates, *Prog. Solid State Chem.*, 28(2000), No. 1-4, p. 201.

[2] Z.M. Sun, Progress in research and development on MAX phases: A family of layered ternary compounds, *Int. Mater. Rev.*, 56(2011), No. 3, p. 143.

[3] N.V. Tzenov and M.W. Barsoum, Synthesis and characterization of Ti_3AlC_2, *J. Am. Ceram. Soc.*, 83(2000), No. 4, p. 825.

[4] M.W. Barsoum, H.I. Yoo, I.K. Polushina, V.Y. Rud', Y.V. Rud', and T. El-Raghy, Electrical conductivity, thermopower, and Hall effect of Ti_3AlC_2, Ti_4AlN_3, and Ti_3SiC_2, *Phys. Rev. B*, 62(2000), No. 15, p. 10194.

[5] P.C. Wingert and C.H. Leung, The development of silver-based cadmium-free contact materials, *IEEE Trans. Compon. Hybrids Manuf. Technol.*, 12(1989), No. 1, p. 16.

[6] M.M. Liu, J.L. Chen, H. Cui, S.H. Liu, X.D. Sun, M. Xie, and X.D. Li, Temperature-driven deintercalation and structure evolution of Ag/Ti_3AlC_2 composites, *Ceram. Int.*, 44(2018), No. 15, p. 18129.

[7] T. El-Raghy, M.W. Barsoum, and M. Sika, Reaction of Al with Ti_3SiC_2 in the 800–1000°C temperature range, *Mater. Sci. Eng. A*, 298(2001), No. 1-2, p. 174.

[8] C.L. Zhou, X.Y. Wu, T.L. Ngai, L.J. Li, S. Ngai, and Z.M. Chen, Al alloy/Ti_3SiC_2 composites fabricated by pressureless infiltration with melt-spun Al alloy ribbons, *Ceram. Int.*, 44(2018), No. 6, p. 6026.

[9] Y. Zhang, Z.M. Sun, and Y.C. Zhou, Cu/Ti_3SiC_2 composite: A new electrofriction material, *Mater. Res. Innovations*, 3(1999), No. 2, p. 80.

[10] J. Zhang, J.Y. Wang, and Y.C. Zhou, Structure stability of Ti_3AlC_2 in Cu and microstructure evolution of Cu–Ti_3AlC_2 composites, *Acta Mater.*, 55(2007), No. 13, p. 4381.

[11] J.X. Ding, W.B. Tian, D.D. Wang, P.G. Zhang, J. Chen, Y.M. Zhang, and Z.M. Sun, Microstructure evolution, oxidation behavior and corrosion mechanism of Ag/Ti_2SnC composite during dynamic electric arc discharging, *J. Alloys Compd.*, 785(2019), p. 1086.

[12] T. Okamoto, Interfacial structure of metal-ceramic joints, *ISIJ Int.*, 30(1990), No. 12, p. 1033.

[13] O.M. Akselsen, Diffusion bonding of ceramics, *J. Mater. Sci.*, 27(1992), No. 3, p. 569.

[14] N. Eustathopoulos, Dynamics of wetting in reactive metal/ceramic systems, *Acta Mater.*, 46(1998), No. 7, p. 2319.

[15] J.R. Lu, Y. Zhou, Y. Zheng, H.Y. Li, and S.B. Li, Interface structure and wetting behaviour of Cu/Ti_3SiC_2 system, *Adv. Appl. Ceram.*, 114(2015), No. 1, p. 39.

[16] T.L. Ngai, W. Zheng, and Y.Y. Li, Effect of sintering temperature on the preparation of Cu–Ti_3SiC_2 metal matrix composite, *Prog. Nat. Sci.: Mater. Int.*, 23(2013), No. 1, p. 70.

[17] Y. Zhou, B. Chen, X. Wang, and C. Yan, Mechanical properties of Ti_3SiC_2 particulate reinforced copper prepared by hot pressing of copper coated Ti_3SiC_2 and copper powder, *Mater. Sci. Technol.*, 20(2004), No. 5, p. 661.

[18] S. Wang, S.Y. Zhu, J. Cheng, Z.H. Qiao, J. Yang, and W.M. Liu, Microstructural, mechanical and tribological properties of Al matrix composites reinforced with Cu coated Ti_3AlC_2, *J. Alloys Compd.*, 690(2017), p. 612.

[19] B.Y. Guan, X. Wang, Y. Xiao, Y.L. Liu, and Q.S. Huo, A versatile cooperative template-directed coating method to construct uniform microporous carbon shells for multifunctional core–shell nanocomposites, *Nanoscale*, 5(2013), No. 6, art. No. 2469.

[20] Q. Wang, B.Y. Wang, Z. Zhang, Y. Zhang, J. Peng, Y. Zhang, and H. Wu, Tailoring yolk–shell FeP@carbon nanoboxes with

engineered void space for pseudocapacitance-boosted lithium storage, *Inorg. Chem. Front.*, 5(2018), No. 10, p. 2605.

[21] P.X. Huang, S.H. Tang, H. Peng, and X. Li, *In situ* synthesis of graphitized-carbon coated $Li_4Ti_5O_{12}$/C anode for high-rate lithium ion batteries, *Mater. Sci. Forum*, 814(2015), p. 358.

[22] J. Ding, W.B. Tian, P. Zhang, M. Zhang, Y.M. Zhang, and Z.M. Sun, Arc erosion behavior of Ag/Ti_3AlC_2 electrical contact materials, *J. Alloys Compd.*, 740(2018), p. 669.

[23] M. Zhang, W.B. Tian, P.G. Zhang, J.X. Ding, Y.M. Zhang, and Z.M. Sun, Microstructure and properties of Ag–Ti_3SiC_2 contact materials prepared by pressureless sintering, *Int. J. Miner. Metall. Mater.*, 25(2018), No. 7, p. 810.

[24] D.D. Wang, W.B. Tian, A.B. Ma, J.X. Ding, C.S. Wang, Y.Y. You, P.G. Zhang, J. Chen, Y.M. Zhang, and Z.M. Sun, Anisotropic properties of Ag/Ti_3AlC_2 electrical contact materials prepared by equal channel angular pressing, *J. Alloys Compd.*, 784(2019), p. 431.

[25] L.M. Pan, J. Gu, W.J. Zou, T. Qiu, H.B. Zhang, and J. Yang, Brazing joining of Ti_3AlC_2 ceramic and 40Cr steel based on Ag–Cu–Ti filler metal, *J. Mater. Process. Technol.*, 251(2018), p. 181.

[26] M.M. Liu, J.L. Chen, H. Cui, X.D. Sun, S.H. Liu, and M. Xie, Ag/Ti_3AlC_2 composites with high hardness, high strength and high conductivity, *Mater. Lett.*, 213(2018), p. 269.